Polyhedron 30 (2011) 178–186

Contents lists available at ScienceDirect

Polyhedron

journal homepage: www.elsevier.com/locate/poly

# Chiral copper–bipyridine complexes: Synthesis, characterization and mechanistic studies on asymmetric cyclopropanation

Wing-Sze Lee [a], Chi-Tung Yeung [a], Kiu-Chor Sham [a], Wing-Tak Wong [b], Hoi-Lun Kwong [a,*]

[a] Department of Biology and Chemistry, City University of Hong Kong, Tat Chee Avenue, Kowloon, Hong Kong SAR, China
[b] Department of Chemistry, The University of Hong Kong, Pokfulam Road, Hong Kong SAR, China

ARTICLE INFO

*Article history:*
Received 21 July 2010
Accepted 12 October 2010
Available online 5 November 2010

*Keywords:*
Chiral bipyridines
Copper–bipyridine complexes
Asymmetric catalysis
Cyclopropanation

ABSTRACT

Chiral bipyridine ligands of different steric properties when reacted with $CuCl_2$ formed orange, yellow or green solids of new copper(II) complexes, [Cu(**L**)$Cl_2$] (**L** = **L2**–**6**), in good yield. Together with [Cu(**L1**)$Cl_2$], these complexes were characterized in solution by UV–Vis spectroscopy and cyclic voltammetry. The complexes give *d*–*d* transitions between 860 and 970 nm, and exhibit one quasi-reversible Cu(II)/Cu(I) couple between +0.405 V and +0.516 V versus NHE. Two of the copper(II) complexes, [Cu(**L5**)$Cl_2$] and [Cu(**L6**)$Cl_2$], and a copper(I) complex of **L1**, [Cu(**L1**)Cl], were characterized by X-ray crystallography. The triflate derivatives of both the Cu(I) and Cu(II) complexes are active catalysts towards the cyclopropanation of ethyl diazoacetate with styrene. The asymmetric induction suffers when the size difference between the alkyl and alkoxyl groups was minimized. The mechanism of the cyclopropanation was studied with kinetic and competition experiments. The rate is first order in catalyst and ethyl diazoacetate, inverse order with styrene and is strongly affected by the counterion.



## 1. Introduction

Copper–diimine complexes have been of great interest in a number of research areas, such as photochemistry [1,2], supramolecular chemistry [3,4] electrochemistry [5,6] and catalysis [7–9]. In enantioselective reactions, chiral versions of the complexes have also been used successfully in catalysis that involved cyclopropanation [10–13] and allylic oxidation [14–16]. The results led us to systematically investigate a family of chiral copper(II) complexes with ligands having different steric properties. Herein, we report the synthesis, spectroscopic characterisation and redox behaviours of a series of copper(II)–bipyridine complexes, as well as their use in the asymmetric cyclopropanation of styrene with ethyl diazoacetate (EDA). X-ray crystal structures for [Cu(**L5**)$Cl_2$] and [Cu(**L6**)$Cl_2$] and a copper(I) complex, [Cu(**L1**)Cl], are described. The results of mechanistic studies and kinetic studies under pseudo-first order conditions on the asymmetric cyclopropanation catalysts are also presented.

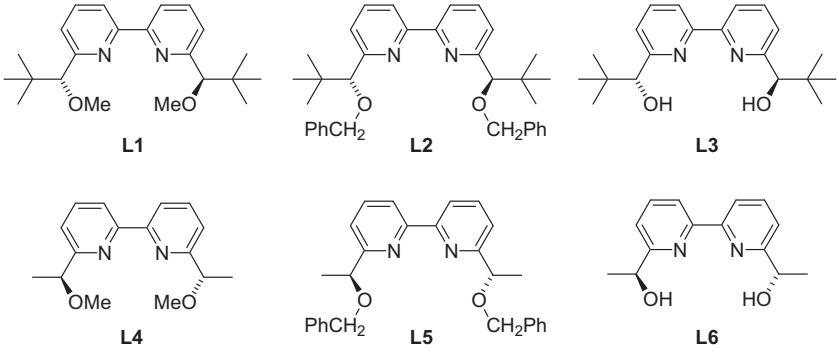


* Corresponding author. Tel.: +852 27887304; fax: +852 27887406.
*E-mail address:* bhhoik@cityu.edu.hk (H.-L. Kwong).

0277-5387/$ - see front matter © 2010 Elsevier Ltd. All rights reserved.
doi:10.1016/j.poly.2010.10.021

## 2. Experimental

### 2.1. General methods

Toluene was distilled under $N_2$ over sodium. Dichloromethane and acetonitrile were distilled over calcium hydride. Diethyl ether and THF were distilled under $N_2$ over sodium/benzophenone. Chemicals were of reagent-grade quality and were obtained commercially. Infrared spectra in the range 500–4000 $cm^{-1}$ using a Nujol matrix or KBr plates were recorded on a Perkin–Elmer Model FTIR-1600 spectrometer. The electronic absorption spectra were measured on a Perkin–Elmer Lambda 19 double-beam UV–Vis-NIR spectrophotometer. $^1H$ and $^{13}C$ NMR spectra were recorded on a Varian 300 MHz Mercury instrument. Positive ion FAB mass spectra as a 3-nitrobenzylalcohol matrix were recorded on a Finnagin MAT 95 spectrometer. ESI-MS were taken by a PE SCIEX API 365 mass spectrometer. Electron ionization mass spectra were recorded on a Hewlett–Packard 5890II GC instrument coupled with a 5970 mass selective detector. Elemental analyses were performed on a Vario EL elemental analyzer. Optical rotations were measured by a JASCO DIP-370 digital polarimeter. Melting points were measured by an electrothermal digital apparatus. The chiral bromopyridine intermediates and bipyridines L1, L3 and L6 were prepared according to the literature procedures [17]. [Cu(**L1**)$Cl_2$] and [Cu(**L1**)Cl] were synthesized according to our previously reported procedure [11].

### 2.2. Synthesis of bipyridines *L2*, *L4* and *L5*

At 70 °C and under $N_2$, to $NiCl_2{\cdot}6H_2O$ (6 mmol, 1.43 g) in degassed DMF (30 ml), triphenylphosphine (24 mmol, 6.30 g) was added to give a blue solution. Zinc powder (13 mmol, 0.87 g) was then added and the resulting mixture was stirred for 1 h, resulting in the formation of a dark-brown mixture. The suitable bromopyridine (5 mmol) in degassed DMF (5 ml) was added slowly and the mixture was stirred for another 3 h. The mixture was then allowed to cool to room temperature and 5% aqueous $NH_3$ (50 ml) was added. The layers were separated, and the aqueous layer was extracted three times with $CH_2Cl_2$ (70 ml × 3). The combined organic layers were washed three times with water (50 ml × 3) and once with brine (50 ml). Drying with $Na_2SO_4$ and removal of the solvent under reduced pressure yielded a pale yellow solid. This was purified by column chromatography (petroleum ether–ethyl acetate) to give a white solid.

#### 2.2.1. Bipyridine *L2*

Yield: 0.66 g (52%); $^1H$ NMR ($CDCl_3$): $\delta$ 1.02 (s, 18H), 4.33 (s, 2H), 4.32–4.50 (m, 4H), 7.27–7.35 (m, 10H), 7.47 (d, 2H, $J$ = 7.5 Hz), 7.81 (t, 2H, $J$ = 7.5 Hz), 8.29 (d, 2H, $J$ = 7.5 Hz); $^{13}C$ NMR ($CDCl_3$): $\delta$ 26.3, 26.3, 26.4, 35.7, 71.3, 90.4, 119.4, 121.6, 121.6, 127.1, 128.0, 136.5, 138.7, 154.8, 159.6. *Anal.* Calc. for $C_{34}H_{40}O_2N_2$: C, 80.28; H, 7.93; N, 5.51. Found: C, 80.48; H, 7.70; N, 5.24%.

#### 2.2.2. Bipyridine *L4*

Yield: 0.38 g (56%); $^1H$ NMR ($CDCl_3$): $\delta$ 1.53 (d, 6H, $J$ = 6.6 Hz), 3.36 (s, 6H), 4.50–4.56 (m, 2H), 7.43 (d, 2H, $J$ = 7.8 Hz), 7.83 (t, 2H, $J$ = 7.8 Hz), 8.33 (d, 2H, $J$ = 7.5 Hz); $^{13}C$ NMR ($CDCl_3$): $\delta$ 22.3, 56.8, 80.8, 119.5, 119.6, 137.3, 155.3, 162.2. *Anal.* Calc. for $C_{16}H_{20}O_2N_2$: C, 70.56; H, 7.40; N, 10.29. Found: C, 70.70; H, 7.38; N, 9.99%.

#### 2.2.3. Bipyridine *L5*

Yield: 0.52 g (49%); $^1H$ NMR ($CDCl_3$): $\delta$ 1.59 (d, 6H, $J$ = 6.6 Hz), 4.47–4.58 (m, 4H), 4.72–4.79 (m, 2H), 7.30–7.37 (m, 10H), 7.54 (d, 2H, $J$ = 7.5 Hz), 7.84 (t, 2H, $J$ = 7.8 Hz), 8.35 (d, 2H, $J$ = 7.5 Hz); $^{13}C$ NMR ($CDCl_3$): $\delta$ 22.7, 70.9, 78.8, 78.9, 119.7, 127.5, 127.6, 128.3, 137.5, 138.3, 155.3, 162.6. *Anal.* Calc. for $C_{28}H_{28}O_2N_2$: C, 79.22; H, 6.65; N, 6.60. Found: C, 79.29; H, 6.54; N, 6.34%.

### 2.3. Procedure for the preparation of [Cu(*L*)$Cl_2$]

Chiral bipyridine **L** (0.4 mmol) in $CH_2Cl_2$ (5 ml) was added drop-by-drop to a solution of $CuCl_2{\cdot}2H_2O$ (0.4 mmol, 0.068 g) in absolute ethanol (5 ml). The mixture was refluxed for a few hours. Addition of ether to the cooled reaction mixture led to the formation of a microcrystalline solid. The mixture was placed in the refrigerator overnight and the microcrystalline solid was filtered and washed with ether.

#### 2.3.1. [Cu(*L2*)$Cl_2$]

Recrystallization from $CH_2Cl_2$/EtOH/$Et_2O$ gave 0.136 g (53%) of an orange solid: *Anal.* Calc. for $CuN_2Cl_2C_{34}H_{40}O_2$: C, 63.49; H, 6.22; N, 4.36. Found: C, 64.10; H, 6.12; N, 4.48%. UV–Vis-NIR spectrum ($CH_2Cl_2$), $\lambda_{max}$ (nm) ($\varepsilon$/$M^{-1}$ $cm^{-1}$): 245 (16 000), 311 (15 000), 390 sh (852), 887 (150); MS (+FAB): 607($M^+$−Cl) and 572 ($M^+$−2Cl).

#### 2.3.2. [Cu(*L3*)$Cl_2$]

Recrystallization from $CH_2Cl_2$/EtOH/$Et_2O$ gave 0.152 g (83%) of a green solid: IR (KBr, $cm^{-1}$): 3268 s; *Anal.* Calc. for $CuN_2Cl_2{\cdot}C_{20}H_{28}O_2{\cdot}(H_2O)$: C, 49.94; H, 6.24; N, 5.83. Found: C, 49.98; H, 6.27; N, 5.79%. UV–Vis-NIR spectrum (MeOH), $\lambda_{max}$ (nm) ($\varepsilon$/$M^{-1}$ $cm^{-1}$): 304 (11 400), 246 (10 700), 257 (9300), 871 (70); MS (API): 390 ($M^+$−HCl−Cl).

#### 2.3.3. [Cu(*L4*)$Cl_2$]

Recrystallization from $CH_2Cl_2$/EtOH/$Et_2O$ gave 0.109 g (67%) of a yellow solid: *Anal.* Calc. for $CuN_2Cl_2C_{16}H_{20}O_2$: C, 47.23; H, 4.92; N, 6.89. Found: 47.57; H, 4.83; N, 7.01%. UV–Vis-NIR spectrum ($CH_2Cl_2$), $\lambda_{max}$ (nm) ($\varepsilon$/$M^{-1}$ $cm^{-1}$): 315 (15 400), 301 (14 500), 246 (12 600), 366 sh (770), 996 (110); MS (+FAB): 370 ($M^+$−Cl) and 335 ($M^+$−2Cl).

#### 2.3.4. [Cu(*L5*)$Cl_2$]

Recrystallization from $CH_2Cl_2$/EtOH/$Et_2O$ gave 0.132 g (59%) of a yellow solid: *Anal.* Calc. for $CuN_2Cl_2C_{28}H_{28}O_2$: C, 60.16; H, 5.01; N, 5.01. Found: 61.13; H, 4.91; N, 5.11%. UV–Vis-NIR spectrum ($CH_2Cl_2$), $\lambda_{max}$ (nm) ($\varepsilon$/$M^{-1}$ $cm^{-1}$): 307 (16 000), 317 (14 900), 246 sh (11 000), 377 sh (738), 980 (130); MS (+FAB): 522 ($M^+$−Cl) and 587 ($M^+$−2Cl).

#### 2.3.5. [Cu(*L6*)$Cl_2$]

Recrystallization from MeOH/$Et_2O$ gave 0.064 g (42%) of a green solid: IR (KBr, $cm^{-1}$): 3534 versus; *Anal.* Calc. for $CuN_2Cl_2C_{14}H_{16}O_2$: C, 44.39; H, 4.23; N, 7.40. Found: 44.44; H, 4.15; N, 7.49%. UV–Vis-NIR spectrum (MeOH), $\lambda_{max}$ (nm) ($\varepsilon$/$M^{-1}$ $cm^{-1}$): 308 (10 300), 258 (12 000), 318 (7900), 438 (100), 860 (70); MS (+FAB): 342 ($M^+$−Cl).

### 2.4. X-ray crystallography analysis for [Cu(*L5*)$Cl_2$], [Cu(*L6*)$Cl_2$] and [Cu(*L1*)Cl]

For [Cu(**L5**)$Cl_2$] and [Cu(**L1**)Cl], diffraction data were obtained on a Rigaku AFC7R diffractometer at 296 and 301 K, respectively. Absorption corrections based on the PSI scans technique were applied on both of these complexes. The structures were solved by using direct methods (SHELXS97) and refined on $F^2$ against all reflections. The absolute configurations of [Cu(**L1**)Cl] at C11 and C17 were found to be *R*, as confirmed by the Flack parameter of 0.000(14). For [Cu(**L6**)$Cl_2$], diffraction data were obtained on a Burker SMART 1000 CCD diffractometer at 298 K. The multi-scan method was applied for absorption correction. The structure was

**Table 1**
Crystallographic data for [Cu(**L5**)$Cl_2$], [Cu(**L6**)$Cl_2$] and [Cu(**L1**)Cl].

| Complex | [Cu(**L5**)$Cl_2$] | [Cu(**L6**)$Cl_2$] | [Cu(**L1**)Cl] |
|---|---|---|---|
| Formula | $C_{28}H_{28}Cl_2CuN_2O_2$ | $C_{14}H_{16}Cl_2CuN_2O_2$ | $C_{22}H_{32}ClCuN_2O_2$ |
| Molecular weight | 558.96 | 378.73 | 455.49 |
| Crystal color, habit | yellow, rod | green, block | brown, rod |
| Crystal dimensions (mm) | 0.12 × 0.07 × 0.07 | 0.22 × 0.22 × 0.10 | 0.07 × 0.21 × 0.23 |
| Crystal system | orthorhombic | trigonal | monoclinic |
| *Lattice* | | | |
| *a* (Å) | 12.947(3) | 10.965(1) | 9.7263(13) |
| *b* (Å) | 25.011(3) | 10.965(1) | 11.3273(14) |
| *c* (Å) | 8.044(4) | 22.247(2) | 11.5636(15) |
| $\alpha$ (°) | 90 | 90.00 | 90 |
| $\beta$ (°) | 90 | 90.00 | 112.837(9) |
| $\gamma$ (°) | 90 | 120.00 | 90 |
| *V* (Å$^3$) | 2604.7(15) | 2316.4(4) | 1174.1(3) |
| Space group | $P2_12_12_1$ (no. 19) | $P3_121$ (no. 144) | $P2_1$ |
| *Z* value | 4 | 6 | 2 |
| $D_{calc}$ (g/cm$^3$) | 1.425 | 1.629 | 1.288 |
| *T* (K) | 301 | 298 | 296(2) |
| Radiation, $\lambda$ (Å) | Mo K$\alpha$, 0.71073 | Mo K$\alpha$, 0.71073 | Mo K$\alpha$, 0.71073 |
| $\mu$ (Mo K$\alpha$) (mm$^{-1}$) | 1.07 | 1.76 | 1.06 |
| $2\theta_{max}$ (°) | 50.0 | 55.0 | 45.0 |
| *F*(0 0 0) | 1156 | 1158 | 480 |
| Reflections: measured/independent/with $I > 2\sigma(I)$ | 2224/2224/689 | 14385/3490/2682 | 3482/3078/2718 |
| $R_{int}$ | 0.000 | 0.040 | 0.022 |
| *R*-factor: $R_1$; *wR* | 0.046; 0.166 | 0.032; 0.070 | 0.033; 0.090 |
| Flack parameter | – | 0.000(14) | 0.000(14) |

solved by using the heavy atoms Patterson method (PATTY) and refined on $F^2$ against all reflections. The absolute configurations of the molecule were found to be *S* for C2 and C13, as confirmed by the Flack parameter of 0.000(14). Crystal data and details of the measurements for these complexes are summarized in Table 1.

### 2.5. Cyclic voltammetry analysis

Cyclic voltammetry was performed using a CH Instruments Electrochemical Workstation CHI750A. Experiments were carried out under nitrogen in a three-electrode cell with glassy-carbon as the working electrode, a Pt-wire as the counter electrode and saturated Ag/$AgNO_3$ as the reference electrode. Ferrocene was used as the internal standard and 0.1 M tetrabutylammonium hexafluorophosphate as a supporting electrolyte. Cyclic voltammograms were scanned at room temperature in the potential range between +0.6 V and −0.2 V at the sweep rate of 0.1 V/s.

### 2.6. Procedure for copper-catalyzed cyclopropanation

Under nitrogen, [Cu(**L**)$Cl_2$] (0.02 mmol), AgOTf (0.04 mmol) and $CH_2Cl_2$ (2 ml) were added to a two-neck round bottom flask and stirred at room temperature for 2 h. The mixture was filtered through a packed filter-paper and styrene (4 mmol) was added. The catalyst was activated by the addition of 0.2 equiv of diazoacetate. Some of the complexes required heating during the activation process. Using a syringe pump, a solution of diazoacetate (1 mmol) in $CH_2Cl_2$ (0.5 ml) was added to the reaction mixture over a period of 4 h. After the addition of diazoacetate, the mixture was allowed to stir for 16 h at room temperature. The solvent was then removed and the crude product obtained was purified by column chromatography (hexane/EtOAc). All the cyclopropanes obtained are known compounds and were characterized by $^1$H NMR, $^{13}$C NMR, IR and GC–MS. The enantiomeric excesses of the cyclopropanes were determined by HPLC with a Daicel Chiralcel OJ column. Absolute configurations were determined by comparing the order of elution with samples of a known configuration [18]. Diastereoselectivities (*cis*/*trans* ratio) were measured by GC with an Ultra 2-crosslinked 5% PhMesilcone (25 m × 0.2 mm × 0.33 μm) column. For competition experiments, an equal amount of styrene (2 mmol) and substituted styrene (2 mmol) was used.

### 2.7. Kinetic experiments (EDA decomposition)

All the kinetics experiments reported here were carried out by the following procedure: to a two-neck round bottom flask were added [Cu(**L1**)Cl] (0.0046 g, 0.01 mmol), degassed chloroform (5.0 ml) and silver(I) salt (0.01 mmol) under nitrogen. The solution was stirred at room temperature for 10 min and filtered through a packed filter paper to another flask containing a solution of chlorobenzene, an internal standard (0.01 M) in degassed chloroform (95 ml). EDA (0.01 mmol) was then added and the reaction was monitored by GC until no EDA was present. For cyclopropanation with styrene, styrene was added together with the internal standard. For the investigation of the counterion, suitable silver salts were used.

## 3. Results and discussion

### 3.1. Ligands and complexes syntheses

The chiral bipyridines **L1**–**6**, having different substituent groups, were prepared either as reported previously (**L1**, **L3** and **L6**) or following a similar synthetic route (**L2**, **L4** and **L5**) [17]. The copper(II) complexes [Cu(**L**)$Cl_2$] (**L** = **L1**–**6**) were obtained in moderate to good yields by the reaction of an equal molar ratio mixture of **L** and $CuCl_2{\cdot}2H_2O$ in dichloromethane–ethanol solution at reflux temperature. All the complexes were air-stable in the solid state and in solution. Elemental analyses indicate that these compounds are 1:1 ligand-to-copper complexes with two chloride ions. The positive ion FAB mass spectra for these complexes show parent ion peaks with masses that matched with the formulas calculated by CHN analysis. The colors of the complexes are different: [Cu(**L1**)$Cl_2$] and [Cu(**L2**)$Cl_2$] are orange; [Cu(**L4**)$Cl_2$] and [Cu(**L5**)$Cl_2$] are yellow; and [Cu(**L3**)$Cl_2$] and [Cu(**L6**)$Cl_2$] are green. Both the orange and yellow colors are unusual for Cu(II) complexes [19]. Copper(I) complexes of these ligands have also been prepared

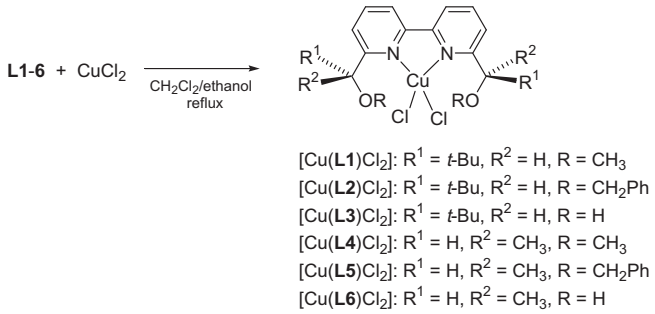


**Scheme 1.** Synthesis of $[Cu(\mathbf{L})Cl_2]$.

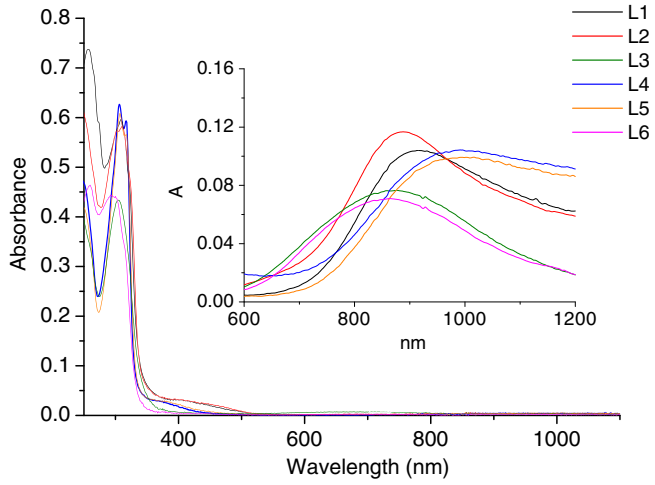


**Fig. 1.** Electronic absorption spectra of (a) $[Cu(\mathbf{L})Cl_2]$ ($\mathbf{L}$ = **L1**–**6**) at a concentration of $3.8 \times 10^{-5}$ M at room temperature ($CH_2Cl_2$ was used for **L1**, **L2**, **L4** and **L5**, MeOH was used for **L3** and **L6**). The inset shows spectra in the region 600–1200 nm at a concentration of $1.0 \times 10^{-3}$ M.

but these are mostly unstable, except for [Cu(**L1**)Cl] which is a reddish brown solid (Scheme 1).

### 3.2. Spectroscopic properties

As the color of the complexes $[Cu(\mathbf{L})Cl_2]$ vary from orange ($\mathbf{L}$ = **L1** and **L2**) to yellow ($\mathbf{L}$ = **L4** and **L5**) to green ($\mathbf{L}$ = **L3** and **L6**), their spectroscopic behaviors were explored. UV–Vis-NIR electronic absorption spectra of $[Cu(\mathbf{L})Cl_2]$ ($\mathbf{L}$ = **L1**–**6**) are shown in Fig. 1. Intense absorption bands at about 252 and 310 nm in the UV-region may be attributed to $\pi$–$\pi^*$ transitions of the bpy ligands [20]. These absorption bands extend to the visible region with different molar absorptivities. For the complexes with **L1** and **L5**, relatively strong absorptions at 406 ($\varepsilon \approx 800\ M^{-1}\ cm^{-1}$) and 377 nm ($\varepsilon \approx 700\ M^{-1}\ cm^{-1}$) were observed respectively. These absorptions are generally believed to originate from LMCT ($Cl^- \rightarrow Cu^{II}$) [20]. For $[Cu(\mathbf{L6})Cl_2]$, the absorption for this transition is weak (~438 nm, $\varepsilon \approx 100\ M^{-1}\ cm^{-1}$). In addition to the above, all the complexes exhibit a very broad band in the lower energy region (>600 nm), tentatively assigned to a Cu(II) d–d transition [20]. Many studies have shown that the energies of these d–d transitions correlate with the copper coordination geometries [21] and that the intensity maximum is shifted to lower energy when the geometry is changed from a regular square pyramid to a regular trigonal bipyramid [21–23]. This was also observed in our study, as $[Cu(\mathbf{L6})Cl_2]$, which is a distorted square pyramid with $\tau = 0.28$ (*vide infra*), absorbed at a higher energy than $[Cu(\mathbf{L5})Cl_2]$ (860 versus 980 nm), which has comparatively more of a trigonal bipyramidal form with $\tau = 0.48$

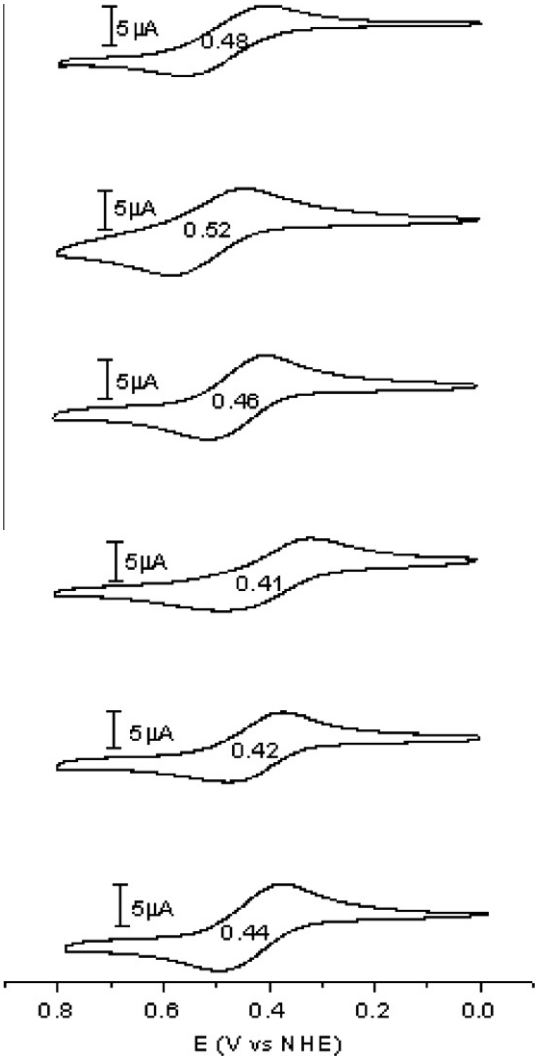


**Fig. 2.** Cyclic voltammograms of $[Cu(\mathbf{L})Cl_2]$ ($\mathbf{L}$ = **L1**–**6** from top to bottom) in acetonitrile with a scan rate of 0.1 V/s. All the potentials were measured against the $Ag/AgNO_3$ reference electrode.

**Table 2**
Cyclic voltammetric parameters for $[Cu(\mathbf{L})Cl_2]$.

| Complex | $E_{1/2}$ (V) | $\Delta E_p$ (mV)[a] | $i_{p,c}/i_{p,a}$[b] |
|---|---|---|---|
| $[Cu(\mathbf{L1})Cl_2]$ | +0.482 | 155 | 1.03 |
| $[Cu(\mathbf{L2})Cl_2]$ | +0.516 | 134 | 0.49 |
| $[Cu(\mathbf{L3})Cl_2]$ | +0.462 | 107 | 1.04 |
| $[Cu(\mathbf{L4})Cl_2]$ | +0.405 | 166 | 0.83 |
| $[Cu(\mathbf{L5})Cl_2]$ | +0.424 | 103 | 1.05 |
| $[Cu(\mathbf{L6})Cl_2]$ | +0.436 | 121 | 1.08 |

[a] Cathodic peak to anodic peak separation.
[b] Ratio of cathodic peak current to anodic peak current.

(*vide infra*). In addition, the absorption at 980 nm for $[Cu(\mathbf{L5})Cl_2]$ may be assigned to the transition of $d_{xz}$ or $d_{yz} \rightarrow d_z^2$ and the absorption at 860 nm for $[Cu(\mathbf{L6})Cl_2]$ may be assigned to the transition of $d_z^2 \rightarrow d_x^2 - y^2$ [21,24]. For $[Cu(\mathbf{L1})Cl_2]$, as reported previously [11], the absorption at 919 nm indicates a pseudo-tetrahedral geometry [25]. Complex $[Cu(\mathbf{L2})Cl_2]$, which has a color similar to $[Cu(\mathbf{L1})Cl_2]$, has an absorption at 887 nm and might also have a tetrahedral geometry. When compared with $[Cu(\mathbf{L6})Cl_2]$ and $[Cu(\mathbf{L5})Cl_2]$, respectively, the similar absorptions of $[Cu(\mathbf{L3})Cl_2]$ and $[Cu(\mathbf{L4})Cl_2]$ possibly indicate similarities in geometries.

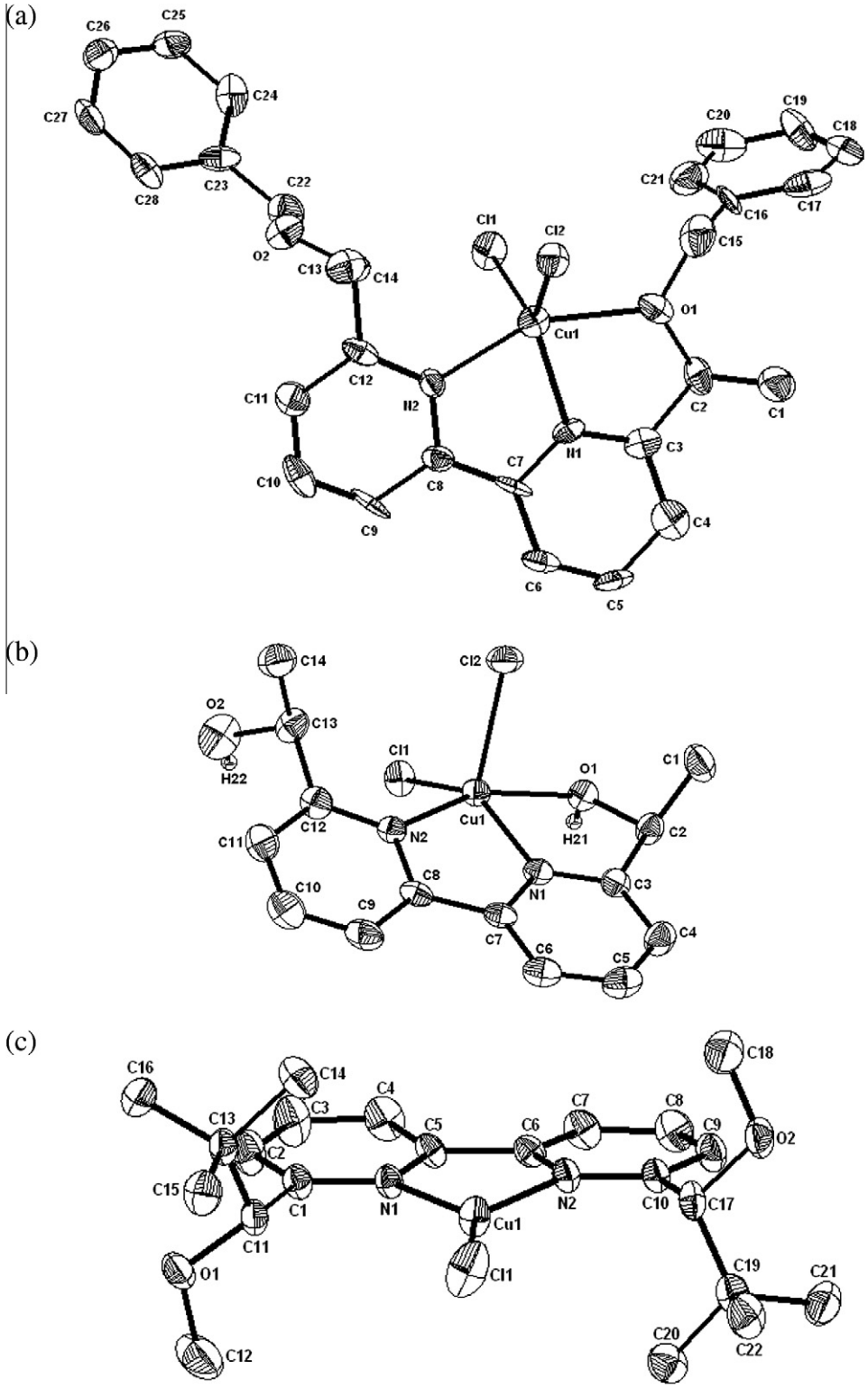


**Fig. 3.** Crystal structures for (a) [Cu(**L5**)$Cl_2$], (b) [Cu(**L6**)$Cl_2$] and (c) [Cu(**L1**)Cl] including the atom numbering schemes. All hydrogen atoms have been omitted for clarity.

### 3.3. Redox behaviour

The redox behaviour of the Cu(II/I) couple in acetonitrile was assessed by cyclic voltammetry. For comparison, the cyclic voltammograms are shown in Fig. 2 and data summarized in Table 2. As the cathodic and anodic peak separations ($\Delta E_p$ = 103 − 166 mV) are larger than those of a fully reversible process ($\Delta E_p$ = 59 mV), and as the cathodic to anodic peak current ratios, $i_{p,c}/i_{p,a}$, deviate from unity, all complexes exhibit quasi-reversible electron transfer behavior.

The $E_{1/2}$ values for the complexes with ligands that contain the bulkier *t*-butyl substituents (**L1**–**3**) are higher than the copper complexes with the less bulky corresponding methyl substituents (**L4**–**6**). This observation provides evidence that the steric

**Table 3**
Selected bond distances and angles for [Cu(**L5**)$Cl_2$], [Cu(**L6**)$Cl_2$] and [Cu(**L1**)Cl].

| | [Cu(**L5**)$Cl_2$] | [Cu(**L6**)$Cl_2$] | [Cu(**L1**)Cl] |
|---|---|---|---|
| Atoms | | | |
| *Bond lengths (Å)* | | | |
| Cu(1)–Cl(1) | 2.311(5) | 2.274(1) | 2.129(3) |
| Cu(1)–Cl(2) | 2.302(5) | 2.424(1) | – |
| Cu(1)–N(1) | 2.009(13) | 1.959(3) | 2.067(6) |
| Cu(1)–N(2) | 2.065(14) | 2.064(3) | 2.054(10) |
| Cu(1)–O(1) | 2.135(13) | 2.095(2) | – |
| *Bond angles (°)* | | | |
| Cl(1)–Cu(1)–Cl(2) | 118.86(19) | 107.99(3) | – |
| Cl(1)–Cu(1)–O(1) | 95.97(37) | 93.27(7) | – |
| Cl(1)–Cu(1)–N(1) | 114.18(144) | 141.28(9) | 138.7(1) |
| Cl(1)–Cu(1)–N(2) | 95.52(40) | 100.37(8) | 140.69(9) |
| Cl(2)–Cu(1)–O(1) | 89.75(40) | 92.13(6) | – |
| Cl(2)–Cu(1)–N(1) | 126.23(39) | 109.98(9) | – |
| Cl(2)–Cu(1)–N(2) | 103.37(40) | 100.55(8) | – |
| O(1)–Cu(1)–N(1) | 76.44(54) | 78.11(12) | – |
| O(1)–Cu(1)–N(2) | 155.58(52) | 157.41(10) | – |
| N(1)–Cu(1)–N(2) | 79.19(57) | 80.00(11) | 80.61(12) |
| *Dihedral angles (°)* | | | |
| N(1)–C(x)–C(y)–N(2) | −9.75(232)<br>$x = 7$, $y = 8$ | −6.14(42)<br>$x = 7$, $y = 8$ | −6.04(48)<br>$x = 5$, $y = 6$ |

bulkiness of **L1**–**3** distorts the copper(II) state and hence makes the complexes easier to reduce than those with ligands that are less bulky. Among the three structurally characterized complexes (*vide infra*), the $E_{1/2}$ for the tetrahedral complex, [Cu(**L1**)$Cl_2$], is higher than that for the square pyramid complex, [Cu(**L6**)$Cl_2$]. The $E_{1/2}$ value for the trigonal bipyramidal complex, [Cu(**L5**)$Cl_2$], is the lowest. The high $E_{1/2}$ value for [Cu(**L1**)$Cl_2$] is most probably due to the minimal alteration to the preferred tetrahedral geometry when the complex is reduced to Cu(I) [23,26,27]. Along the same line, in the case of the two five-coordinated complexes, the higher $E_{1/2}$ value of [Cu(**L6**)$Cl_2$] can be attributed to be the smaller change in its square pyramidal geometry during reduction from Cu(II) to Cu(I), whereas the lower $E_{1/2}$ value of [Cu(**L5**)$Cl_2$] likely reflects a significant change in geometry upon reduction.

### 3.4. Structural characterization

The crystal structures of [Cu(**L5**)$Cl_2$], [Cu(**L6**)$Cl_2$] and [Cu(**L1**)Cl] are shown in Fig. 3a–c. Selected bond lengths and angles are listed in Table 3. The copper(II) centres of both [Cu(**L5**)$Cl_2$] and [Cu(**L6**)$Cl_2$] are five-coordinated and have a distorted trigonal bipyramidal geometry: one of the nitrogen atoms N(1) of the bipyridine ligand and two chloride ions occupy the equatorial plane while the oxygen O(1) atom and the remaining nitrogen atom N(2) are axial. The marked difference between these two structures and the previously reported [Cu(**L1**)$Cl_2$] [11] demonstrate that the coordination environment is affected by the steric property of the ligand.

In the structure of [Cu(**L5**)$Cl_2$], the copper–nitrogen bond distances for the two nitrogen atoms are different (Cu(1)–N(1) = 2.009(13) Å, Cu(1)–N(2) = 2.065(14) Å) but they are within the range generally found for other copper(II) bipyridine complexes [28,29]. The copper–chloride bonds are 2.311(5) and 2.302(5) Å and the copper–oxygen bond is 2.135(13) Å. The bite angle of 79.2° made by the bipyridine ligand and copper is small when compared with that of 83.0° for [Cu(**L1**)$Cl_2$] [11]. As the O(1)–Cu(1)–N(2) angle is 155.6°, the O–Cu–N linkage for the complex is not perfectly linear. The bond angles around the Cu(1) centre Cl(1)–Cu(1)–Cl(2), Cl(1)–Cu(1)–N(1) and Cl(2)–Cu(1)–N(1) are 118.9°, 114.2° and 126.2°, respectively. As the sum of these angles is 359.3°, the equatorial plane of the complex is almost planar. As the degree of distortion in the geometry of a five-coordinated complex can be represented by the value of its trigonality $\tau$ index [30], the $\tau$ index of 0.48 for [Cu(**L5**)$Cl_2$] reflects the distorted nature of its complex.

[Cu(**L6**)$Cl_2$] also has a distorted trigonal bipyramidal geometry similar to [Cu(**L5**)$Cl_2$]: one of the nitrogen atoms N(1) of the bipyridine ligand and two chloride ions occupy the equatorial plane while the oxygen atom O(1) and the remaining nitrogen atom N(2) are axial. The copper–nitrogen bond distances (Cu(1)–N(1) = 1.959(3) Å; Cu(1)–N(2) = 2.064(3) Å) are slightly shorter than those of [Cu(**L5**)$Cl_2$]. The two copper–chloride bonds are different (Cu(1)–Cl(1) = 2.274(1) Å and Cu(1)–Cl(2) = 2.424(1) Å). The copper–oxygen bond is 2.095(2) Å. The bite angle of 80.0° made by the bipyridine ligand and copper is comparable to that of [Cu(**L5**)$Cl_2$]. The O(1)–Cu(1)–N(2) angle of 157.4° (Table 2) shows the O–Cu–N linkage is not perfectly linear. The bond angles for Cl(1)–Cu(1)–Cl(2), Cl(1)–Cu(1)–N(1) and Cl(2)–Cu(1)–N(1) are 108.0°, 141.3° and 110.0°, respectively. As the angles around the copper sum up to 359.3°, the equatorial plane of the complex is almost planar. Given its $\tau$ index of 0.28, the structure of [Cu(**L6**)$Cl_2$] is more distorted and closer to a square pyramid.

The copper(I) centre of [Cu(**L1**)Cl] is three-coordinated and has a Y-shaped planar geometry, with the metal ion surrounded by two pyridine nitrogen atoms and one chloride anion. The copper–nitrogen bond distances are 2.054(10) and 2.067(6) Å. These bond distances are slightly longer than the copper–nitrogen bond distances for other achiral three-coordinate copper(I) phenanthroline complexes. The bite angle of 80.6° made by the bipyridine ligand and copper is small when compared with the value of 82.9° cited in the literature [31]. The bond angles for Cl(1)–Cu(1)–N(1) and Cl(1)–Cu(1)–N(2) are 138.7° and 140.7°, respectively. The angles around copper sum up to be 360° which suggests that the complex is planar in geometry. The copper–chloride bond distance is 2.129 Å. There are a few examples of three-coordinate Y-shaped copper(I) complexes reported in the literature [32–34]. The large difference in geometry between [Cu(I)(**L1**)Cl] and [Cu(I)(**L1**)$Cl_2$] probably explains the quasi-reversible nature of the Cu(II)/Cu(I) redox couple.

### 3.5. Catalytic asymmetric cyclopropanation

The use of [Cu(**L**)$Cl_2$] (**L** = **L2**–**6**) in the cyclopropanation of styrene with EDA was studied and the results are summarized in Table 4. The active form of the catalyst was generated *in situ* by reacting 2 mol% of [Cu(**L**)$Cl_2$] with AgOTf, which was then filtered and reacted with a few equivalents of EDA to reduce the copper(II) species to copper(I). Copper catalysts generated from **L1**–**5** required no heating and were much more easily activated than the one from **L6**, which required heating at 40 °C for a few minutes. As **L6** has the lowest $E_{1/2}$ value, the result is consistent with our observation on the correlation between the Cu(II)/Cu(I) redox potential of the copper(II) chloride complex and the $E_{1/2}$ value.

All these copper–bipyridine complexes were active catalysts, producing cyclopropyl esters in yields between 85% and 99% (entries 1–6). The best results in both enantioselectivity and diastereoselectivity (*trans*:*cis* = 80:20) were achieved with **L1**, which gave 90% ee and 82% ee for *trans* and *cis*-isomers, respectively (entry 1). *Trans*/*cis* ratios ranged from 66:34 to 80:20 (entries 1–6). When **L2** and **L3** were employed, the absolute configurations of the cyclopropane esters were found to be (1*R*, 2*R*) and (1*R*, 2*S*) for the *trans* and *cis* isomers, respectively, similar to **L1**. Employment of **L4**–**6** resulted in the opposite absolute configurations (*trans* = 1*S*, 2*S*; *cis* = 1*S*, 2*R*). This can be attributed to the use of ligands with opposite configuration, thus the sense of asymmetric induction observed is also consistent with **L1** [11]. In general, better enantioselectivity and *trans*/*cis* ratio are observed with the *t*-butyl series of ligands. Decreasing the size difference between the alkyl group and the alkoxy/hydroxy group has a negative effect. The

**Table 4**
Asymmetric cyclopropanation of styrene with ethyl diazoacetate, catalyzed by [Cu(**L**)(OTf)$_2$].

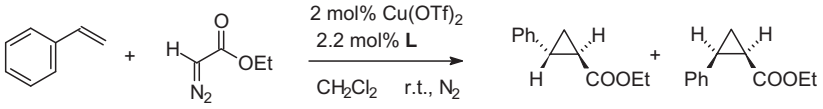


| Entry[a] | Ligand | Yield (%)[b] | *trans*/*cis* | % ee. (config.)[c] | |
|---|---|---|---|---|---|
| | | | | *trans* | *cis* |
| 1 | **L1** | 85 | 80:20 | 90 (1*R*, 2*R*) | 82 (1*R*, 2*S*) |
| 2 | **L2** | 86 | 76:24 | 83 (1*R*, 2*R*) | 57 (1*R*, 2*S*) |
| 3 | **L3** | 92 | 74:26 | 73 (1*R*, 2*R*) | 38 (1*R*, 2*S*) |
| 4 | **L4** | 88 | 66:34 | 30 (1*S*, 2*S*) | 25 (1*S*, 2*R*) |
| 5 | **L5** | 92 | 66:34 | 43 (1*S*, 2*S*) | 23 (1*S*, 2*R*) |
| 6 | **L6** | 99 | 70:30 | 44 (1*S*, 2*S*) | 26 (1*S*, 2*R*) |

[a] Diazoacetate (0.2 equivalent) was used for the reduction of the Cu(II) catalysts before the start of the cyclopropanation reaction.
[b] Isolated yield after column chromatography.
[c] Enantiomeric excesses were determined by HPLC with a Daicel Chiralcel OJ column, and the absolute configurations were determined by comparing the order of elution of samples with a known configuration [18].

**Table 5**
Catalytic asymmetric cyclopropanation with [Cu(**L1**)X] as the catalyst.

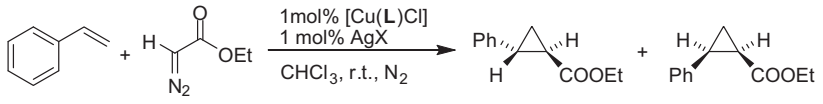


| Entry | AgX | Solvent | *trans*:*cis* | % ee (*trans*)[a] | % ee (*cis*)[a] | Yield %[b] |
|---|---|---|---|---|---|---|
| 1 | | $CHCl_3$ | 80:20 | 90 (1*R*, 2*R*) | 82 (1*R*, 2*S*) | 67 |
| 2 | AgOTf | $CH_2Cl_2$ | 79:21 | 91 (1*R*, 2*R*) | 85 (1*R*, 2*S*) | 68 |
| 3 | | Toluene | 83:17 | 92 (1*R*, 2*R*) | 78 (1*R*, 2*S*) | 70 |
| 4 | | THF | 82:18 | 93 (1*R*, 2*R*) | 85 (1*R*, 2*S*) | 76 |
| 5 | | $CH_3CN$ | – | – | – | – |
| 6 | $AgPF_6$ | $CHCl_3$ | 75:25 | 86 (1*R*, 2*R*) | 85 (1*R*, 2*S*) | 88 |
| 7 | | THF | 75:25 | 79 (1*R*, 2*R*) | 70 (1*R*, 2*S*) | 54 |
| 8 | $AgBF_4$ | $CHCl_3$ | 71:29 | 87 (1*R*, 2*R*) | 83 (1*R*, 2*S*) | 65 |
| 9 | | THF | 75:25 | 91 (1*R*, 2*R*) | 84 (1*R*, 2*S*) | 74 |
| 10 | $AgSbF_6$ | $CHCl_3$ | 74:26 | 85 (1*R*, 2*R*) | 83 (1*R*, 2*S*) | 56 |
| 11 | | THF | 76:24 | 90 (1*R*, 2*R*) | 86 (1*R*, 2*S*) | 43 |
| 12 | $AgClO_4$ | $CHCl_3$ | – | – | – | – |

[a] Enantiomeric excesses were determined by HPLC with a Daicel Chiralcel OJ column, and the absolute configurations were determined by comparing the order of elution of samples with a known configuration [18].
[b] Isolated yield after chromatography.

group on the oxygen has a relatively small effect on the enantioselectivity, probably because of the flexibility of the group and its distance away from the metal centre.

### 3.6. Effect of anion and competition experiments

The use of a silver salt to generate the active catalyst provides an easy way to study the effect of the counter ion. Since **L1** gives the best results and the copper(I) complex is the active form of the catalyst and requires no activation, [Cu(**L1**)Cl] was used as the precursor for our further study. The results with different counterions and different solvents are listed in Table 5. With triflate as the anion, *trans*/*cis* ratios, enantioselectivies and yields in different solvents of different polarity were similar (entries 1–4). No significant solvent effect was observed. However, when the coordinating solvent acetonitrile was used, no reaction occurred (entry 5). Catalysts with $^-$OTf, $BF_4^-$, $PF_6^-$ and $SbF_6^-$ as counterions gave similar *trans*/*cis* ratios, enantioselectivities and isolated yields, no matter whether the reaction took place in chloroform or THF (entries 1, 4, 6–11). These results suggest the existence of a common intermediate for the catalysts with different counterions. For the catalyst with $ClO_4^-$, no reaction took place (entry 12), just like $Cl^-$. This is probably due to the strong coordination of the perchlorate ion to the metal center.

The role of the counterion was further investigated by a competition experiment with substituted styrenes. With [Cu(**L1**)X] (X = $^-$OTf, $PF_6^-$, $BF_4^-$ and $SbF_6^-$ as the catalyst, competitions were carried out in either chloroform or THF. In all cases the reaction rates increased with electron-donating substituted styrenes, i.e. the 4-methoxy- and 4-methylstyrenes, while the electron-withdrawing substituted styrenes, such as 4-chloro- and 3-nitrostyrenes, decreased the reaction rate. In chloroform, good $\sigma$ correlations were obtained with $\rho = -1.35$ for $^-$OTf (Fig. 4), $-1.36$ for both $BF_4^-$ and $SbF_6^-$ and $-1.65$ for $PF_6^-$ (Figs. S1–S3). The negative value of $\rho$ indicates the formation of an electrophilic metal–carbene complex intermediate. The similarity in $\rho$ values obtained with catalysts having different counterions, together with the similarity in enantioselectivities obtained with these catalysts, provide evidence that the counterion is not involved in the active intermediate.

### 3.7. Kinetic rate law

Kinetic studies for the copper-catalyzed cyclopropanation of olefins have been reported previously [35–38]. These studies were

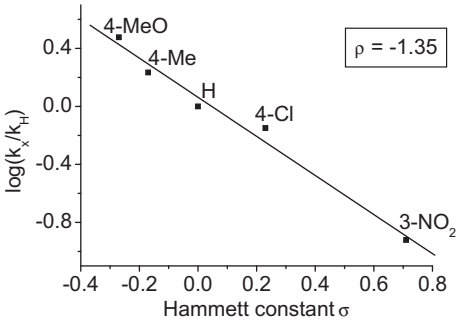


**Fig. 4.** Hammett plot for the cyclopropanation of styrene with EDA in $CHCl_3$ using [Cu(**L1**)OTf] as the catalyst.

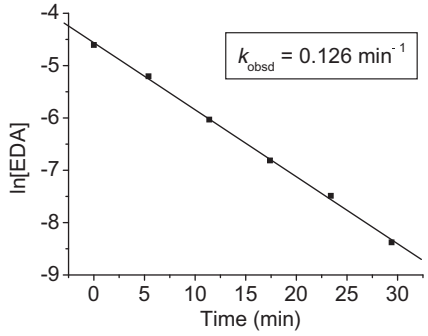


**Fig. 5.** EDA decomposition catalyzed by [Cu(**L1**)OTf].

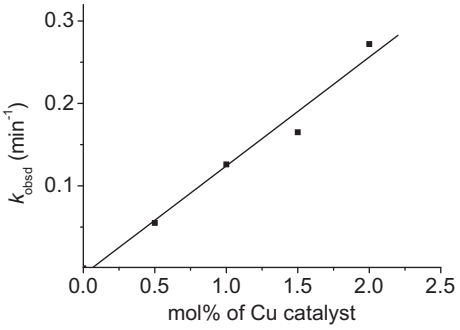


**Fig. 6.** Variation of $k_{obsd}$ versus $[Cu]_{total}$ for EDA decomposition using [Cu(**L1**)OTf].

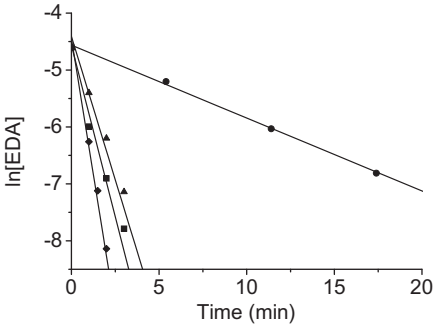


**Fig. 7.** EDA decomposition in the absence of olefin, catalyzed by [Cu(**L**)X] (X = $^{-}$OTf (●), $BF_4^-$ (▲), $PF_6^-$ (■) and $SbF_6^-$ (♦)).

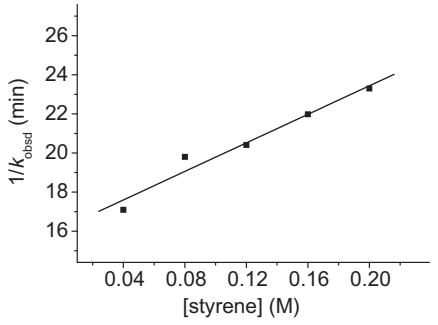


**Fig. 8.** Variation of $k_{obsd}$ versus different concentrations of styrene for EDA decomposition using 1 mol% of [Cu(**L1**)OTf].

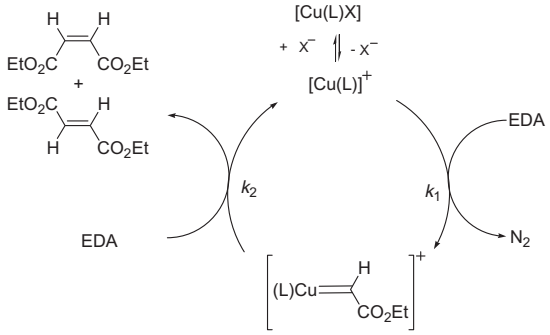


**Scheme 2.**

based on achiral catalysts while we employed chiral catalysts [39]. In the absence of styrene, the rates of EDA decomposition were found to be first order in both [EDA] (Fig. 5) and $[Cu]_{total}$ (Fig. 6), similar to the previous study by Pérez et al. [37,38]. A comparison of the $k_1$ values indicated our catalyst ($k_1$ = 658 $M^{-1}$ $min^{-1}$) is more active than the reported Cu(I)Bp catalyst (where Bp = dihydridibis(1-pyrazoyl)borate) ($k_1$ = 52 $M^{-1}$ $min^{-1}$) [37,38]. With catalysts having different counterions, the rates of EDA decomposition were also found to be affected strongly by the counterions (Fig. 7). EDA decomposition rates were the fastest for $SbF_6^-$ (1.91 $min^{-1}$), slower for $BF_4^-$ (1.01 $min^{-1}$) and $PF_6^-$ (1.18 $min^{-1}$), and slowest for $^{-}$OTf (0.126 $min^{-1}$). These results seem to indicate the presence of an equilibrium between the catalyst and the counterion. With these results, a scheme similar to the one proposed by Pérez et al. is proposed for EDA decomposition (Scheme 2).

In the presence of excess styrene, the reaction rates were found to decrease with [styrene]. A plot of $1/k_{obsd}$ versus [styrene] is linear (Fig. 8). The rate law for cyclopropanation under pseudo-first order conditions is therefore

$$\text{Rate} = \frac{k_1[\text{Cu}]_{\text{total}}[\text{EDA}]}{1 + K[\text{styrene}]}$$

The equilibrium constant $K$ is calculated to be 2.4. The relatively small value obtained here when compared with reported value with Cu(I)Bp ($K$ = 77 ± 29) [38] indicates that [Cu(**L**)OTf] is mostly in the catalytically active form during cyclopropanation. This means more concentrated styrene solutions can be used with our catalyst. Previously Kochi et al. [35] had also observed similar binding and showed catalytically effective copper(I) species were deactivated by the multiple coordination of olefin, which in turn inhibited the EDA decomposition.

### 3.8. Mechanism of copper-catalyzed asymmetric cyclopropanation

A general mechanistic scheme with copper-catalyzed cyclopropanation, similar to that proposed by Pérez and his co-workers [38], is shown in Scheme 3. The active catalyst here, a 14-electron fragment of [Cu(**L1**)]$^+$, can undergo two possible reactions: (i) with styrene to form a copper–olefin complex, which has a retardation

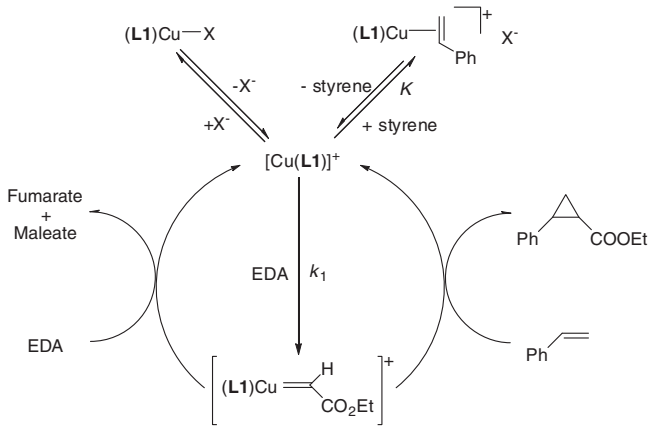


**Scheme 3.**

effect on EDA decomposition; and (ii) with EDA to form a copper–carbene intermediate, which subsequently reacts with styrene to form cyclopropane or with another equivalent of EDA to form diethyl fumarate and maleate as byproducts.

## 4. Conclusions

In summary, we have described the synthesis and characterizations of a family of copper(II) complexes, [Cu(**L**)$Cl_2$], derived from chiral bipyridines **L1**–**6**. Our data show the steric properties of the ligands not only affect the colour and coordination geometries but also the redox properties. [Cu(**L**)$Cl_2$] are isolated as either orange, yellow or green solids. As revealed by X-ray crystallography, [Cu(**L5**)$Cl_2$] and [Cu(**L6**)$Cl_2$] have distorted trigonal bipyramidal geometries that are different from that of [Cu(**L1**)$Cl_2$]. Cyclic voltammetry data show that complexes with ligands containing bulkier groups (**L1**–**3**) are more easily reduced than those with ligands containing less bulky group (**L4**–**6**). The $^-$OTf, $PF_6^-$, $BF_4^-$ and $SbF_6^-$ forms of the complex can function as catalysts for the asymmetric cyclopropanation of styrene with EDA. Kinetic and mechanistic studies suggest that a 14-electron species is the active catalyst in the carbene transfer reaction.

## Acknowledgements

Financial support from the Hong Kong Research Grants Council GRF (CityU 101108) and the Area of Excellence Scheme established under the University Grants Committee of the Hong Kong SAR, China (Project No. AoE/P-10/01) and the City University of Hong Kong are gratefully acknowledged.

## Appendix A. Supplementary data

CCDC 158090, 732089 and 732090 contains the supplementary crystallographic data for [Cu(L1)Cl], [Cu(L5)Cl2] and [Cu(L6)Cl2]. These data can be obtained free of charge via http://www.ccdc.cam.ac.uk/conts/retrieving.html, or from the Cambridge Crystallographic Data Centre, 12 Union Road, Cambridge CB2 1EZ, UK; fax: (+44) 1223-336-033; or e-mail: deposit@ccdc.cam.ac.uk. Supplementary data associated with this article can be found, in the online version, at doi:10.1016/j.poly.2010.10.021.

## References

[1] D.R. McMillin, K.M. McNett, Chem. Rev. 98 (1998) 1201.
[2] R.M. Williams, L. De Cola, F. Hartl, J.-J. Lagref, J.-M. Planeix, A. De Cian, M.W. Hosseini, Coord. Chem. Rev. 230 (2002) 253.
[3] C. Kaes, A. Katz, M.W. Hosseini, Chem. Rev. 100 (2000) 3553.
[4] R. Ziessel, Coord. Chem. Rev. 216 (2001) 195.
[5] A. Ion, M. Buda, J.-C. Moutet, E. Saint-Aman, G. Royal, I. Gautier-Luneau, M. Bonin, R. Ziessel, Eur. J. Inorg. Chem. (2002) 1357.
[6] S. Kume, M. Kurihara, H. Nishihara, Inorg. Chem. 42 (2003) 2194.
[7] L.A. Adrio, K.K. Hii, Chem. Commun. (2008) 2325.
[8] J. Niu, H. Zhou, Z. Li, J. Xu, S. Hu, J. Org. Chem. 73 (2008) 7814.
[9] C. Ricardo, L.M. Matosziuk, J.D. Evanseck, T. Pintauer, Inorg. Chem. 48 (2009) 16.
[10] K. Ito, S. Tabuchi, T. Katsuki, Synlett (1992) 5755.
[11] H.-L. Kwong, W.-S. Lee, H.-F. Ng, W.-H. Chiu, W.-T. Wong, J. Chem. Soc., Dalton Trans. (1998) 1043.
[12] R. Rios, J. Liang, M.M.-C. Lo, G.C. Fu, Chem. Commun. (2000) 377.
[13] D. Lötscher, S. Rupprecht, H. Stoeckli-Evans, A. von Zelewsky, Tetrahedron: Asymm. 11 (2000) 4341.
[14] A.V. Malkov, M. Bella, V. Langer, P. Kočovský, Org. Lett. 2 (2000) 3047.
[15] W.-S. Lee, H.-L. Kwong, H.-L. Chan, W.-W. Choi, L.-Y. Ng, Tetrahedron: Asymm. 12 (2001) 1007.
[16] D.R. Boyd, N.D. Sharma, L. Sbircea, D. Murphy, T. Belhocine, J.F. Malone, S.L. James, C.C.R. Allen, J.T.G. Hamilton, Chem. Commun. (2008) 5535.
[17] C. Bolm, M. Ewald, M. Felder, G. Schlingloff, Chem. Ber. 125 (1992) 1169.
[18] H. Fritschi, U. Leutenegger, A. Pfaltz, Helv. Chim. Acta 71 (1988) 1553.
[19] G.G. Mohamed, N.E.A. El-Gamel, Spectrochim. Acta A 61 (2005) 1089.
[20] M. Ghosh, P. Biswas, U. Flörke, K. Nag, Inorg. Chem. 47 (2008) 281.
[21] A.B.P. Lever, Inorganic Electronic Spectroscopy, second ed., Elsevier, Amsterdam, 1984.
[22] G. Murphy, P. Nagle, B. Murphy, B. Hathaway, J. Chem. Soc., Dalton Trans. (1997) 2645.
[23] B.J. Hathaway, in: G. Wilkinson, R.D. Gillard, J.A. McCleverty (Eds.), Comprehensive Coordination Chemistry, vol. 5, Pergamon, Oxford, 1987, p. 534.
[24] P. Biswas, S. Dutta, M. Ghosh, Polyhedron 27 (2008) 2105.
[25] W.M. Davis, A. Zask, K. Nakanishi, S.J. Lippard, Inorg. Chem. 24 (1985) 3737.
[26] R. Mukherjee, in: J.A. McCleverty, T.J. Meyer (Eds.), Comprehensive Coordination Chemistry II, vol. 6, Elsevier, Amsterdam, 2004, p. 747.
[27] H. Börzel, P. Comba, K.S. Hagen, C. Katsichtis, H. Pritzkow, Chem. Eur. J. 6 (2000) 914.
[28] C. O'Sullivan, G. Murphy, B. Murphy, B. Hathaway, J. Chem. Soc., Dalton Trans. (1999) 1835.
[29] R.D. Willett, G. Pon, C. Nagy, Inorg. Chem. 40 (2001) 4342.
[30] A.W. Addison, T.N. Rao, J. Reedijk, J. van Rijn, G.C. Verschoor, J. Chem. Soc., Dalton Trans. (1984) 1349.
[31] M. Munakata, M. Maekawa, S. Kitagawa, S. Matsuyama, H. Masuda, Inorg. Chem. 28 (1989) 4300.
[32] A.J. Pallenberg, K.S. Koenig, D.M. Barnhart, Inorg. Chem. 34 (1995) 2833.
[33] A.J. Blake, P. Hubberstey, W.-S. Li, D.J. Quinlan, C.E. Russell, C.L. Sampson, J. Chem. Soc., Dalton Trans. (1999) 4261.
[34] B.A. Gandhi, O. Green, J.N. Burstyn, Inorg. Chem. 48 (2007) 3816.
[35] R.G. Solomon, J.K. Kochi, J. Am. Chem. Soc. 95 (1973) 3300.
[36] M.M. Díaz-Requejo, P.J. Pérez, M. Brookhart, J.L. Templeton, Organometallics 16 (1997) 4399.
[37] M.M. Díaz-Requejo, M.C. Nicasio, P.J. Pérez, Organometallics 17 (1998) 3051.
[38] M.M. Díaz-Requejo, T.R. Belderrain, M.C. Nicasio, F. Prieto, P.J. Pérez, Organometallics 18 (1999) 2601.
[39] For the derivation of the rate law, see supporting information.